

## MULTIPLE SCATTERING OF WAVES BY A PAIR OF GRAVITATIONALLY STRATIFIED FLUX TUBES

SHRAVAN M. HANASOGE<sup>1,3</sup> AND PAUL S. CALLY<sup>2</sup>

<sup>1</sup> Max-Planck-Institut-für-Sonnensystemforschung, 37191 Katlenburg-Lindau, Germany  
<sup>2</sup> Centre for Stellar and Planetary Astrophysics, Monash University, Victoria 3800, Australia  
Received 2008 December 6; accepted 2009 March 9; published 2009 May 4

### ABSTRACT

We study the near-field coupling of a pair of flux tubes embedded in a gravitationally stratified environment. The mutual induction of the near-field *jackets* of the two flux tubes can considerably alter the scattering properties of the system, resulting in sizable changes in the magnitudes of scattering coefficients and bizarre trends in the phases. The dominant length scale governing the induction zone turns out to be approximately half the horizontal wavelength of the incident mode, a result that fits in quite pleasantly with extant theories of scattering. Higher- $\beta$  flux tubes are more strongly coupled than weaker ones, a consequence of the greater role that the near-field jacket modes play in such tubes. We also comment on the importance of incorporating the effects of multiple scattering when studying the effects of mode absorption in plage and interpreting related scattering measurements. That the near field plays such an important role in the scattering process lends encouragement to the eventual goal of observationally resolving subwavelength features of flux tubes using techniques of helioseismology.

*Key words:* hydrodynamics – Sun: helioseismology – Sun: interior – Sun: oscillations – waves

### 1. INTRODUCTION

An outstanding issue in solar physics concerns the accurate constraining of the internal constitution of sunspots. Since we are unable directly image the interior, we study the solar acoustic wave field in and around sunspots and attempt to comprehend these observations through theories of wave interactions. An example of such an effort is the first putative detection of downflows underneath sunspots by Duvall et al. (1996), who analyzed the solar wave field using methods of time–distance helioseismology (Duvall et al. 1993). In the Sun, observations have almost always been more plentiful than theory. Of late, the importance of developing theoretical and computational methods to aid the interpretation of observations of solar magnetism has risen to the fore. A considerable body of computational work has recently focused on understanding the nature of wave interactions in magnetized environments (e.g., Khomenko & Collados 2006; Cameron et al. 2007; Hanasoge 2008). Complementary to such efforts, we attempt here to develop further the theory of flux tube related multiple scattering, probably ubiquitously present on the Sun but has, for the most part, been studiously ignored in the past due to the many challenges involved in modeling such interactions. On another front, it is important to place bounds on the degree of wave absorption and scattering by the plage for it tells us how much energy is transmitted to the corona and could help explain the complex frequency dependence of acoustic mode line widths (e.g., Bogdan et al. 1996; Hindman & Jain 2008). Because plage comprises ensembles of compactly packed thin flux tubes, the interaction with waves possibly lies in the multiple scattering regime.

In linear theory, when a wave encounters an anomaly of some sort, it is scattered at constant frequency, with the resultant wave field being broadly classified into near- and far-field components. The far field consists of propagating modes that transport some fraction of the incident mode energy away from the scatterer. The near field is more complex, comprising a number of nonpropagating horizontally evanescent waves, that

arise when the displacements of the anomaly due to the external wave buffeting cannot be matched by the set of eigenfunctions of the propagating modes. In the case of stratified flux tubes in the Sun, the set of  $p$ -mode eigenfunctions at constant frequency is an incomplete basis, requiring a supplementary set, an uncountably infinite continuum in fact, of these evanescent near-field functions to complete the basis. The problem is exacerbated when the displacement eigenfunctions of the scatterer gain complexity.

The mathematics required to address the near field in the case of thin flux tubes was set down by Bogdan & Cally (1995), who termed this nonpropagating sheath of waves as an “acoustic jacket” that envelopes flux concentrations. The uncountable continuum of jacket modes arises as a consequence of an infinitely deep lower boundary, required in order to allow the tube modes to disappear into the solar interior. Unfortunately, numerically computing the near-field jacket in this scenario is all but impossible because of various formidable integrals in the equations. In order to arrive at an analogous but more tractable problem, Barnes & Cally (2000) introduced an artificial lower boundary, leading to a discrete and countably infinite number of near-field modes. More recently, Hanasoge et al. (2008) adopted the model of Barnes & Cally (2000) and estimated the magnitude of the near-field jacket and the single scattering by an isolated thin flux tube. They attempted to model the observations of Duvall et al. (2006), who characterized the scattering of  $f$  modes by magnetic flux elements. However, magnetic elements are known to consist of a number of tightly packed flux tubes, all likely within the near fields of each other. Thus, the single scattering assumption may not be entirely accurate when interpreting these measurements.

The presence of a large body of theory to draw upon makes it easier to proceed toward an understanding of the importance of multiple scattering. When a pair of flux tubes lie in the proximity of each other, their near fields communicate and depending on the separation, can dramatically alter the nature of the scatter. Thus, accounting for the mutual induction of near fields is rather important when studying plage or other closely spaced scatterers. Bogdan & Fox (1991), when considering a pair of

<sup>3</sup> Visiting academic at Indian Institute of Astrophysics, Bangalore, India.

flux tubes at a series of separations in an unstratified medium, found evidence for three different scattering regimes that they termed multiple, coherent, and incoherent. The nomenclature points to differences in the degree of coupling between the two flux tubes, with the incoherent regime no different from isolated body scattering and the multiple regime, substantially different. Subsequently, Keppens et al. (1994) studied ensembles of flux tubes and found that the degree of absorption was greater in “spaghetti” models than monoliths, pointing to a way of discerning the differences between the two.

These efforts have been restricted to unstratified media, mainly due to the considerable mathematical complexity that stratification injects. With the addition of gravity, the external driver and the flux tube displacement eigenfunctions assume distinct and more complicated forms, possibly destroying a number of resonances hitherto possible in the unstratified case. Furthermore, purely analytical techniques cease to be of utility, even when considering single scattering, let alone its multiple counterpart. When studying mode mixing due to thin flux tubes, Hanasoge et al. (2008) were forced to apply a number of methods of linear algebra in order to reliably estimate scattering coefficients and the near-field jacket. On the other hand, multiple scattering is a bit more of a challenge since one must simultaneously determine the wave fields of a number of disparate scatterers, all the while keeping in mind that each scattering coefficient is defined according to a coordinate system centered on that specific scatterer. Fortunately, the theoretical machinery to study these sorts of problems has been developed decades ago, in the context of fluid mechanics by, e.g., Kagimoto & Yue (1986) and Linton & Evans (1990). We adopt these methods in our calculations in order to determine the degree of mode mixing and scattering from a two-tube system. Please note that in the discussions below, the terms “near field,” “acoustic jacket,” and “envelope of evanescent modes” are used interchangeably. This paper is organized as follows. We describe the stratification and basic aspects of the flux tube model in Section 2. The method of Kagimoto & Yue (1986) in the context of interacting thin flux tubes is discussed in Section 3. The scattering coefficients derived through the application of these techniques for the two-tube system for different incident modes are presented in Section 4. Finally, we summarize and conclude in Section 5.

## 2. MODEL

The background structure in this calculation, adapted from Bogdan et al. (1996) and Hanasoge et al. (2008), is an adiabatically stratified, truncated polytrope with index  $m = 1.5$ , gravity  $\mathbf{g} = -2.775 \times 10^4 \text{ cm s}^{-2} \hat{z}$ , reference pressure  $p_0 = 1.21 \times 10^5 \text{ g cm}^{-1} \text{ s}^{-2}$ , and reference density  $\rho_0 = 2.78 \times 10^{-7} \text{ g cm}^{-3}$ , such that the pressure and density variations are given by,

$$p(z) = p_0 \left( -\frac{z}{z_0} \right)^{m+1}, \quad (1)$$

and

$$\rho(z) = \rho_0 \left( -\frac{z}{z_0} \right)^m. \quad (2)$$

We utilize a right-handed cylindrical coordinate system in our calculations, with coordinates  $\mathbf{x} = (r, \theta, z)$  and corresponding unit vectors  $(\hat{r}, \hat{\theta}, \hat{z})$ . The photospheric level of the background model is at  $z = 0$ , with the upper boundary placed at a depth of  $z_0 = 392 \text{ km}$ . Following Barnes & Cally (2000), we introduce

a lower boundary at a depth of 98 Mm. The displacement potential  $\Psi(\mathbf{x}, t)$  describing the oscillation modes ( $t$  is time) is required to enforce zero Lagrangian pressure perturbation boundary conditions at both boundaries. This upper boundary condition is reflective in nature and therefore, possibly not very realistic. The incoming  $p_n$ -mode, a plane wave, which expanded in cylindrical coordinates (e.g., Gizon et al. 2006) has a displacement eigenfunction,  $\Psi_{\text{inc}}$ , of the form

$$\Psi_{\text{inc}} = \sum_{m=-\infty}^{\infty} i^m J_m(k_n^p r) \Phi_p(k_n^p; s) e^{i[m\theta - \omega t]}, \quad (3)$$

where,

$$\Phi_p(k_n^p; s) = s^{-1/2-\mu} N_n \left[ C_n^p M_{\kappa_n^p, \mu} \left( \frac{sv^2}{\kappa_n^p} \right) + M_{\kappa_n^p, -\mu} \left( \frac{sv^2}{\kappa_n^p} \right) \right]. \quad (4)$$

The various symbols in Equations (3) and (4) are

$$\mu = \frac{m-1}{2}, \quad v^2 = \frac{m\omega^2 z_0}{g}, \quad k_n^p = \frac{v^2}{2\kappa_n^p z_0}, \quad (5)$$

$\omega$  the angular frequency of oscillation,  $s = -z/z_0$ ,  $J_m(w)$ , the Bessel function of order  $m$  and argument  $w$ , and  $M_{\kappa, \mu}(w)$ , the Whittaker function (e.g., Whittaker & Watson 1963) with indices  $\kappa$ ,  $\mu$ , and argument  $w$ . The eigenvalue  $\kappa_n^p > 0$  and constant  $C_n^p$  characterizing the mode are obtained through the procedure described in Appendix A of Hanasoge et al. (2008). The  $n = 0$  mode corresponds to the surface gravity or the  $f$  mode, while  $n > 0$  represents the acoustic  $p_n$  mode. Note that the lower boundary results in a finite sized box and hence places a restriction on the number of  $p$  modes that can fit in this domain. The term  $N_n$  is the normalization constant for the mode, defined as

$$N_n = \left[ \int_1^{\infty} \left[ C_n^p M_{\kappa_n^p, \mu} \left( \frac{v^2 s}{\kappa_n^p} \right) + M_{\kappa_n^p, -\mu} \left( \frac{v^2 s}{\kappa_n^p} \right) \right]^2 ds \right]^{-1/2}. \quad (6)$$

The near-field eigenfunctions are also solutions to the same differential equation that governs the propagating modes:

$$\zeta_n(\kappa_n^J; s) = s^{-1/2-\mu} \left[ C_n^J M_{-i\kappa_n^J, \mu} \left( \frac{iv^2}{\kappa_n^J} s \right) + M_{-i\kappa_n^J, -\mu} \left( \frac{iv^2}{\kappa_n^J} s \right) \right]. \quad (7)$$

As can be seen, the only difference between the form of the propagating and evanescent mode eigenfunctions is the fact that the roots are now imaginary. In order to determine the roots, we perform a high-resolution search for eigenvalues  $\kappa_n^{p,J}$  and constants  $C_n^{p,J}$ ; the task is relatively easy for the propagating mode parameters but is reasonably difficult for the jacket modes because the eigenvalues may be very finely spaced (Appendix A of Hanasoge et al. 2008). Subsequently, tables of the propagating and jacket modes are precomputed at a range of frequencies. Computations of Whittaker functions over large parameter spaces are fairly nontrivial; we use a number of CERNLIB routines to accomplish all these tasks.

### 2.1. Flux Tube

Applying the approximations listed in Section 2 of Bogdan et al. (1996), a thin flux tube carrying a magnetic flux of  $\Phi_f = 3.88 \times 10^{17} \text{ Mx}$ , with constant plasma- $\beta$  everywhere

inside the tube is embedded in the polytrope. The thin flux tube approximation,

$$b(s) \approx \sqrt{\frac{8\pi p(s)}{1 + \beta}}, \quad \pi R^2(s) \approx \frac{\Phi_f}{b(s)}, \quad (8)$$

where  $b(s)$  and  $R(s)$  are the magnetic field and the radius of the tube at depth  $s$ , is shown to be accurate to better than a percent in the truncated polytrope situated below  $z = -z_0$  or  $s = 1$  (Bogdan et al. 1996). Note that the magnetic flux associated with the tube is held constant—different values of  $\beta$  therefore result in different  $b(s)$  and  $R(s)$ . The constant- $\beta$  property of the tube follows from the assumption that thin flux tubes are for all practical purposes in thermal and radiative equilibrium with the external medium.

### 2.2. Oscillations of the Tube

For the cases addressed here, we treat only horizontal kink motions of the flux tube ( $\xi_{\perp}(\omega, s)$ ), caused by impinging  $m = \pm 1$  modes (e.g., Bogdan et al. 1996). The  $m = \pm 1$  modes affect the tube oscillations according to the differential equation

$$\left[ \omega^2 z_0 + \frac{2gs}{(1 + 2\beta)(m + 1)} \frac{\partial^2}{\partial s^2} + \frac{g}{1 + 2\beta} \frac{\partial}{\partial s} \right] \xi_{\perp} = \frac{2(1 + \beta)}{1 + 2\beta} \omega^2 z_0 \frac{\partial \Psi_{\text{inc}}}{\partial x}, \quad (9)$$

where  $x = r \cos \theta$ . The scattered wave field is computed by matching the horizontal components of the motion of the flux tube to the external oscillation velocities. The manner in which this is accomplished is detailed in the following section.

## 3. METHOD

Consider a system of randomly distributed flux tubes. The scattered wave field around tube  $i$  with the origin of the coordinate system located at the center of the upper boundary of the tube is given by

$$\phi_i^S = - \sum_{m=-1}^1 \left[ \sum_{n=0}^{n_p} \alpha_{mn}^i \Phi_n(\kappa_n^p; s) H_m^{(1)}(k_n^p r_i) e^{im\theta_i} + \sum_{n=n_p+1}^N \alpha_{mn}^i \zeta_n(\kappa_n^J; s) K_m(k_n^J r_i) e^{im\theta_i} \right], \quad (10)$$

where  $\zeta_n$  are near-field eigenfunctions,  $\Phi_n$  describe the propagating  $p$ -modes,  $H_m^{(1)}(x)$  and  $K_m(x)$  are Hankel and K-Bessel functions of order  $m$  acting on argument  $x$ , respectively.  $n_p$  denotes the number of propagating mode eigenfunctions (a finite number due to the presence of the lower boundary) and the rest corresponding to the evanescent jacket modes. Also note that the  $m$  summation is truncated, since thin flux tube theory applies only to interactions with  $|m| \leq 1$  waves. Following Kagemoto & Yue (1986), we write this in matrix form:

$$\phi_i^S = \sum_n A_{in}^T \Psi_{in}^S, \quad (11)$$

where  $A_m$  is a vector (of size  $3 \times 1$ ) of scattering coefficients for tube  $i$  and mode  $n$ . The matrix  $\Psi_{in}^S$  (size  $3 \times n_z$ , with  $n_z$  being

the number of points in the  $z$  grid) contains the partial wave expansions in terms of  $H_m^{(1)}$ ,  $K_m$ . In particular, the elements of  $A$ ,  $\Psi$  are

$$A_{in} = -(\alpha_{-1n}^i \quad \alpha_{0n}^i \quad \alpha_{1n}^i)^T, \quad (12)$$

$$(\Psi_{in}^S)_{cd} = H_{c-2}^{(1)}(k_n^p r_i) \Phi_n(\kappa_n^p; s_d) \quad (n \leq n_p), \quad (13)$$

$$(\Psi_{in}^S)_{cd} = K_{c-2}(k_n^J r_i) \zeta_n(\kappa_n^J; s_d) \quad (n > n_p), \quad (14)$$

where  $s_d$  is the  $d$ th point along the  $s$ -axis, and the indices  $c, d$  run from  $[1, 3]$  and  $[1, n_z]$ , respectively. As described in the introductory section, the challenge in computing the wave field interactions lies in simultaneously solving for the scattering coefficients of all the tubes. Tubes that are placed sufficiently far from each other can only interact via the far-field propagating modes since the evanescent jacket has a spatial decay scale of a wavelength or so. Thus, the coupling is reasonably weak since the amplitude of the expanding far-field modal ring falls rapidly with distance from the scatterer. Stronger interactions occur when tubes lie within each other's near-field induction zones, for the evanescent modes of one influence the tube oscillations on the other and vice-versa. Fairly significant changes in the scattering cross-sections are a consequence of this phenomenon. Thus, to capture this effect, we must compute the wave field around each tube and project its influence on the neighboring flux elements. Since the wave field around each tube is written in a coordinate system centered along its axis, suitable coordinate transformations must be performed. For this purpose, we employ Graf's addition formulae, which transform cylindrical wave functions between coordinate systems (e.g., Abramowitz & Stegun 1964):

$$H_m^{(1)}(k_n^p r_i) e^{im(\theta_i - \gamma_{il})} = \sum_{d=-\infty}^{\infty} H_{m+d}^{(1)}(k_n^p R_{il}) J_d(k_n^p r_l) e^{id(\pi - \theta_l + \gamma_{il})}, \quad (15)$$

$$K_m(k_n^J r_i) e^{im(\theta_i - \gamma_{il})} = \sum_{d=-\infty}^{\infty} K_{m+d}(k_n^J R_{il}) I_d(k_n^J r_l) e^{id(\pi - \theta_l + \gamma_{il})}, \quad (16)$$

where  $I_m(x)$  is a Bessel-I function of order  $m$  acting on argument  $x$ . These equations show how to expand an outgoing scattered wave function from tube  $i$  in terms of the incident mode waves of tube  $l$ . Here,  $R_{il}$  is the distance between the centers and  $\gamma_{il}$  is the angle that the line between the centers of the tubes subtends at the  $x$ -axis of the tube  $i$  (shown graphically in Figure 1). This relation shows how the scattered wave field from  $i$  acts as an incident wave on  $l$ .

Written in matrix form

$$\Psi_{in}^S = \mathbf{T}_{il}^n \Psi_{ln}^I, \quad (17)$$

where  $\mathbf{T}$  is the transformation operator that relates the scattered wave field of tube  $i$  to the resultant incident field on  $l$ . We use Equations (15) and (16) to build  $\mathbf{T}$ ; the precise distribution of elements is listed in Appendix A. Note that the index  $n$  that appears in Equation (17) denotes a specific modal order, while the superscripts  $I$  and  $S$  represent the incident and scattered wave expansions, respectively. Recalling that Equation (11) contains the contributions of various near- and far-field waves

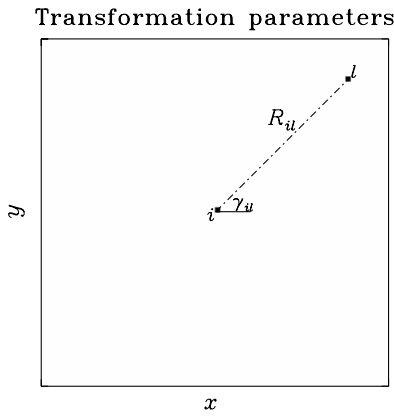


**Figure 1.** Transformation parameters of Equations (15) and (16) shown graphically. The tubes  $i, l$  are separated by a distance  $R_{il}$ , with the line joining their centers inclined at angle  $\gamma_{il}$  to the  $x$ -axis of tube  $i$ . Note that  $\gamma_{li} = \pi - \gamma_{il}$ .

and collecting all the  $n$ 's, we have

$$\phi_{i|l} = \sum_n A_{in}^T \mathbf{T}_{il}^n \Psi_{ln}^I. \tag{18}$$

Equation (18) tells us how much the scattered wave field of tube  $i$  acts as an incident field on  $l$ . Summing up the contributions from the scattered wave fields of all the other flux tubes (except itself, of course) and the zeroth order incident wave, the total incident wave field at  $l$  is given by

$$\phi_l^I = \sum_n \left( \phi_{0|ln} + \sum_{i=1, i \neq l}^N A_{in}^T \mathbf{T}_{il}^n \Psi_{ln}^I \right) \tag{19}$$

$$= \sum_n \left( a_{ln}^T + \sum_{i=1, i \neq l}^N A_{in}^T \mathbf{T}_{il}^n \right) \Psi_{ln}^I, \tag{20}$$

and  $\phi_{0|ln} = a_{ln}^T \Psi_{ln}^I$ , where  $a_{ln}^T$  is a vector of coefficients representing the zeroth order incident wave mode of order  $n$ , acting on tube  $l$ . The determination of the amplitudes of the off-axis incident modes is described in Appendix B. Note that  $a_{ln}$  and  $A_{ln}$  have the same matrix sizes; the former refers to the zeroth order incident wave whereas the latter contains the net scattering terms. Finally, to close the equations, we use the diffraction transfer matrix approach of, e.g., Kagemoto & Yue (1986) to relate the total incident coefficients to the scattered ones. In effect, we generate a matrix  $\mathbf{B}_l$  that acts on the incident wave field at  $l$  and produces the scattering coefficients. We know the total incident wave field at  $l$ : it is given by Equation (20). And since  $\mathbf{A}_l$  is the vector of scattering coefficients as seen by the coordinate system centered on  $l$ , the following relation must hold:

$$\mathbf{A}_l = \mathbf{B}_l \phi_l^I, \tag{21}$$

or,

$$\mathbf{A}_l = \mathbf{B}_l \left( \mathbf{a}_l + \sum_{i=1, i \neq l}^N \mathbf{T}_{il}^T \mathbf{A}_i \right), \tag{22}$$

where we have the following relations:

$$\mathbf{a}_l = a_{l0} \quad a_{l1} \quad a_{l2} \quad \dots^T, \tag{23}$$

$$\mathbf{A}_l = A_{l0} \quad A_{l1} \quad A_{l2} \quad \dots^T, \tag{24}$$

$$\mathbf{T}_{il} = \begin{pmatrix} T_{il}^0 & 0 & 0 & \dots & 0 \\ 0 & T_{il}^1 & 0 & \dots & 0 \\ 0 & 0 & T_{il}^2 & \dots & 0 \\ \dots & \dots & \dots & \dots & \dots \\ 0 & 0 & \dots & 0 & T_{il}^N \end{pmatrix}. \tag{25}$$

(26)

The matrix  $\mathbf{B}_l$  is constructed as follows. The scattering into all other modes is computed for each incident mode  $(m, n)$ . This includes both propagating  $p_n$  modes and near-field-type incident waves (the Bessel-I functions). Thus,  $\mathbf{B}_l$  contains a full description of the scattering of any given incident mode  $(m, n)$  into any  $(m', n')$  for tube  $l$ . More details are described in Appendix A.

Finally, we discuss the means applied to study the simple case of two interacting thin flux tubes 1, 2. Proceeding from Equation (22) we have

$$\mathbf{A}_1 = \mathbf{B}_1 (\mathbf{a}_1 + \mathbf{T}_{21}^T \mathbf{A}_2), \tag{27}$$

$$\mathbf{A}_2 = \mathbf{B}_2 (\mathbf{a}_2 + \mathbf{T}_{12}^T \mathbf{A}_1), \tag{28}$$

$$\mathbf{A}_1 = \mathbf{B}_1 (\mathbf{a}_1 + \mathbf{T}_{21}^T \mathbf{B}_2 [\mathbf{a}_2 + \mathbf{T}_{12}^T \mathbf{A}_1]), \tag{29}$$

$$[\mathbf{I} - \mathbf{B}_1 \mathbf{T}_{21}^T \mathbf{B}_2 \mathbf{T}_{12}^T] \mathbf{A}_1 = \mathbf{B}_1 \mathbf{a}_1 + \mathbf{B}_1 \mathbf{T}_{21}^T \mathbf{B}_2 \mathbf{a}_2. \tag{30}$$

We precompute the  $\mathbf{B}$  matrices for a number of different incident mode frequencies and plasma- $\beta$  values. Finally, having constructed the transformation matrices  $\mathbf{T}$  at a series of tube separations, we apply the standard MATLAB least-squares algorithm (backslash command) to solve Equation (30) for  $\mathbf{A}_1$  and then for  $\mathbf{A}_2$ .

#### 4. DISCUSSION

There are two important issues that must be dealt with before presenting the results. The first concerns the noninclusion of the  $m = 0$  scattering mode. In an isolated body case, the scattering in each  $m$  mode can be cleanly separated, and there is no mechanism by which different  $m$  modes can communicate. This may be attributed to the identification of one primary cylindrical coordinate system (presumably centered around the tube). With multiple closely spaced tubes, this uniqueness is lost and there is now unrestricted modal mixing, among wave numbers and indirectly, between the  $m$ . For example, consider the following chain of events: an  $m = 1$  wave strikes tube 1. According to the axis around tube 1, only a scattered  $m = 1$  wave has been released. However, seen by the coordinate system centered on tube 2 is a mixture of scattered *and* incident  $m = \pm 1, 0$  waves, setting off tube displacements and scattering in all three modes. These scattered waves are then seen by tube 1 as a mixture of  $m = 0, \pm 1$ , resulting in the excitation of the three components. Thus, having started with an  $m = 1$  mode, we now have oscillations and scattering in the  $m = \pm 1, 0$  modes. Moreover, a spatially asymmetric positioning of the tubes destroys the  $m = \pm 1$  scattering equality for a given tube. Symmetries once

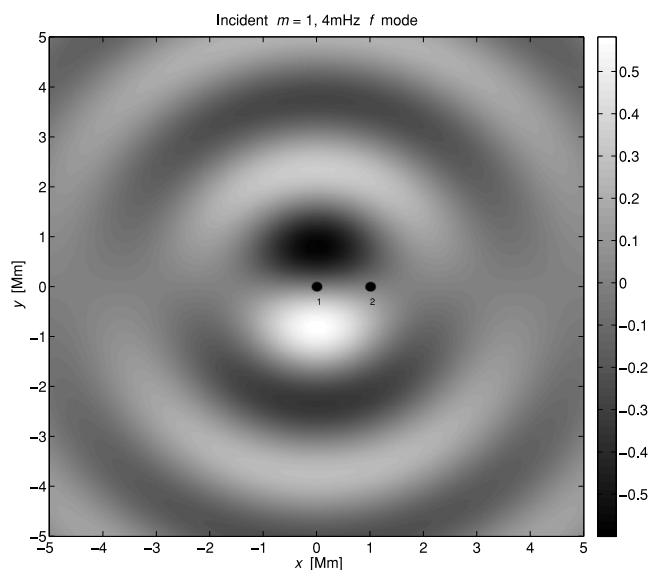


**Figure 2.** Example of an incident  $m = 1$  wave:  $\Psi_{\text{inc}} = i J_1(k_0^p r) e^{i\theta}$ . Tube 1 always sees the incident wave, whereas with increasing separation, tube 2 sees less and less of it. Note that the presence of the second tube kills the  $m = \pm 1$  symmetry when the tubes are close to each other. The symmetry is restored for wide tube separations, at which point, both tubes are practically isolated bodies.

prevalent in the case of an isolated body are now broken, and the degrees of scattering freedom have multiplied. The implication derived from this argument is that by just modeling the  $m = \pm 1$  scattering, we are probably significantly underestimating the degree of scatter. The  $m = 0$  scattering has not been modeled because of difficulties faced in setting up satisfactory boundary conditions.

The second issue relates to the replacement of a discrete countably infinite set of jacket modes to a small, finite subset. What physics have we lost in forcing the problem into this zone of tractability? Although we have verified that the jacket modes used in the calculations are able to fully capture the displacement eigenfunctions of the flux tube, it is not apparent that this form of partial basis completeness (partial because the full basis of jacket modes is countably infinite) is a sufficient criterion. This is certainly an issue that affects the believability of the scattering coefficients although precisely how the coefficients are altered is entirely unclear. Perhaps we must wait for a numerical solution to the partial differential equations in order to verify these results.

Having stated these caveats, we are ready to view the outcome of the two-tube scattering calculations. First, we consider the interaction of a pair of identical flux tubes at different separations with incident waves. The angle between the tubes is set to  $\gamma_{12} = 0$ , meaning that the tubes lie on the  $x$ -axes of the coordinate systems of each other (see Figure 1). Undoubtedly, there will be large changes in the scattering coefficients at different angles; for now we stick to this simple case, and leave further exploration of the parameter space to future endeavors. A pictorial representation of an incoming  $f$ -mode with respect to the flux tubes 1, 2 is shown in Figure 2. The results of these interactions are shown in Figure 3. A number of conclusions may be drawn. (1) The strongest coupling is between the  $f$  mode and the flux tube; there is a rapid fall off with increasing radial order. The  $f$ - $f$  scattering coefficients are almost an order of magnitude larger than the  $p_1$ - $f$  counterparts, as seen in Figure 3. This implies that the scattering matrix is diagonally dominant. However, although not shown here, the scattering

coefficient for  $p_n$ - $p_n$  also falls very rapidly with increasing  $n$ , meaning that the dominant interactions are restricted to the  $f$  mode. (2) The length scale of the region occupied by the near-field region is well approximated by  $\pi/k_n^p$ , where  $2\pi/k_n^p$  is the horizontal wavelength of the incident  $p_n$  mode. This is hardly a surprising result, since it is well known that the far-field imaging limit is bounded from below by half the imaging wavelength (e.g., Gizon & Birch 2004); it serves however as a sanity check and indicates that the calculations are not entirely incorrect. Thus, to resolve the structure of the flux tube at finer scales, we must somehow utilize the information present in the near field. (3) The scattering coefficients attain large values at small flux tube separations (Figure 3); this has a number of consequences for wave absorption in plage. A system of  $N$  closely spaced flux tubes thus turns into a glutinous mass of scatterers and can no longer be interpreted as a collection of  $N$  isolated bodies. (4) The phases of the scattered waves exhibit highly unpredictable trends, even more so than the magnitudes of the scattering coefficient (Figure 4). (5) Higher- $\beta$  flux tubes have more extended jackets than their lower- $\beta$  counterparts; this may be attributed to the fact that when matching tube displacement eigenfunctions to the external waves, the jacket modes play a more significant role in the former case. The last point is further illustrated by the upper two panels of Figure 5 which show the isolated body displacements  $\xi_{\perp}$  of the tubes at plasma- $\beta = 0.1, 1$ . The fact that a larger number of kinks are seen in the higher- $\beta$  tube means a larger number of jacket modes must crowd the near-field region, resulting in stronger coupling between the tubes. The lower two panels of Figure 5 demonstrate the stark differences between the isolated body and near-field coupled tube displacements; the structure, the number of nodes, and the amplitude of the eigenfunction are seen to greatly increase when the jackets of the tubes are able to communicate. This is the very premise of multiple scattering.

We also briefly investigate the interactional behavior of a pair of nonidentical flux tubes in Figure 6. Because the magnetic flux in each tube is held constant (see Section 2.1), the two tubes which have differing plasma- $\beta$  of 0.1, 1 also are of different radii, commensurate with Equation (8). The scattering coefficient trends are unremarkable, showing differences in structure from those of Figure 3 but not possessing any noticeable features. Despite the differences in the flux tube geometries, the coupling remains strong and continues to adhere to the half-wavelength rule-of-thumb near-field dimension. Lastly, in Figure 7, we graph the components of the wave field with the upper panels showing the tubes strongly interacting (a separation distance of 1.085 Mm) while the isolated body case is displayed in the lower panel. In the strong interaction case, the near-field lobes of the two tubes are seen to be in communication, the scattering in one tube significantly influencing the other through this medium. The far fields in both cases are outward spirals, transporting some of the incident mode energy away from the scene of scattering.

Based on these results, how are we to interpret the Hankel measurements of phase shifts and absorption in plage and around active regions? From this simplified model, it is evident that mode mixing between the  $m$  and wave numbers, and multiple scattering are not effects easily swept aside or ignored. However, one aspect that must be borne in mind is that due to stochastic wave excitation in the Sun, the theoretically predicted stark symmetry breaking between the  $\pm m$  seen in the scattering coefficients will probably be significantly moderated. Essentially, the measurements can only retrieve the properties

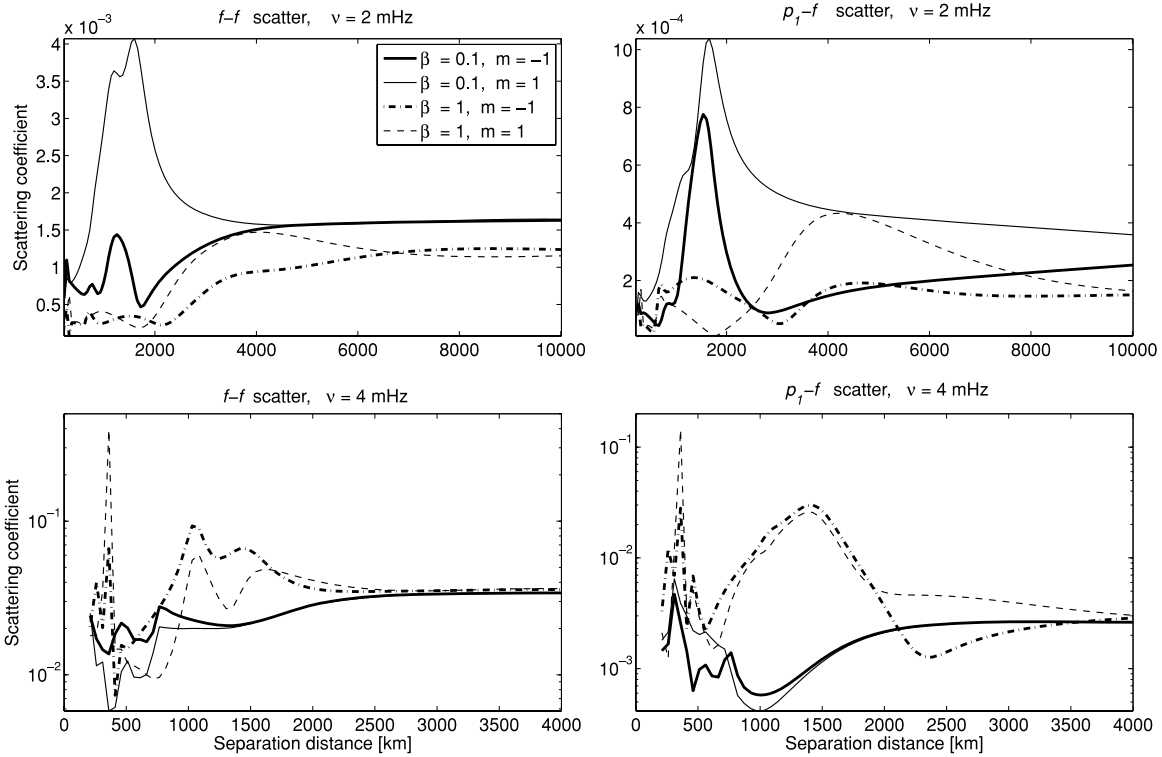


**Figure 3.** Mode-mixing and scattering computed for  $f$  and  $p_1$  incident waves at two different frequencies and azimuthal orders  $m = \pm 1$  for a pair of flux tubes at a number of separations. These are the coefficients written according to the coordinate system centered around tube 1, the tube that encounters the untransformed zeroth order incident mode. Note that the symmetry of the  $m = \pm 1$  scattering coefficients are destroyed due to the presence of tube 2; this symmetry is regained when the separation becomes large enough that tube 1 can be considered an isolated body. Clear signs of multiple scattering are observed for separations comparable to about half the horizontal wavelength at the surface ( $\sim \pi/k_n^p$ ) of the incident waves, which are 11.04 and 2.76 Mm for the  $f$  modes and 25.76 and 6.44 Mm for the  $p_1$  modes at 2 and 4 mHz, respectively. The degree of scatter exhibits a complex behavior at small separations and more importantly, shows rather large deviations from the isolated body values. Note also the differences between the  $m = \pm 1$  modes; the presence of the second flux tube destroys any symmetries with respect to these two  $m$  waves. Also of interest is the fact that the  $\beta = 1$  flux tubes couple via the near field more strongly than the low- $\beta$  tubes; this is presumably because the displacement eigenfunction exhibits more depth structure in the former, requiring a greater participation of the near-field modes, and thereby resulting in stronger coupling (see Figure 5).

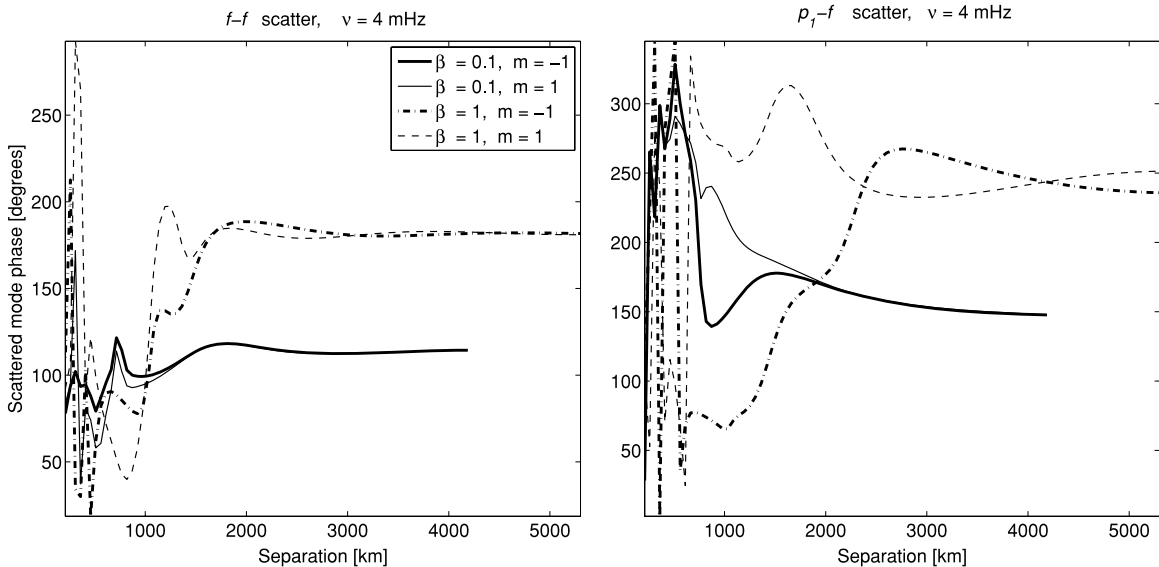


**Figure 4.** Phases of the scattered  $f$  mode. The parameter space is similar to that explored in Figure 3. No clear pattern is seen, indicating that interpreting the phases in a multiply scattered wave field is quite a nontrivial affair.

of the interactions between waves propagating in random directions and the tubes, resulting in an azimuthal average. Furthermore, flux tubes in the Sun are in constant motion due to the jostling by the dynamic granulation field; this may result in another form of averaging in the scatter.

When contemplating the sticky issue of understanding the observations, it is first important to acknowledge that the theory presented here is likely not directly applicable to the solar situation because it is unable to account for the effects of rapidly flaring flux tubes (with radii larger than a

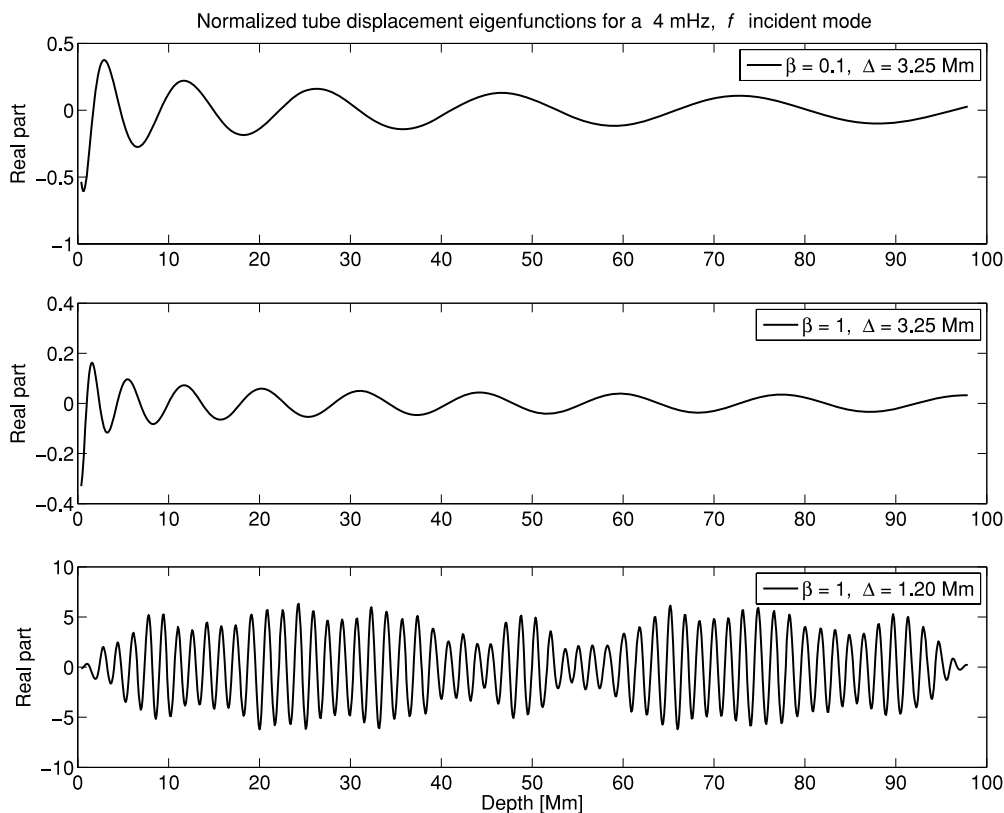


**Figure 5.** Real parts of the normalized tube displacement eigenfunction ( $\xi_{\perp}/k_r^p$ ) for flux tube 1 for  $\beta = 0.1, 1$ , and separations,  $\Delta = 1.20, 3.25$  Mm. At this frequency, tubes at a separation distance of 3.25 Mm can be considered§ isolated bodies. The first aspect take note of is that the displacement eigenfunction of the isolated body  $\beta = 0.1$  tube has fewer nodes and therefore less structure in depth than the  $\beta = 1$  tube (upper two panels). Consequently, a greater near-field participation is required to successfully match the  $\beta = 1$  tube displacements with the external wave eigenfunctions, resulting in a more diverse near field than the  $\beta = 0.1$  case. Second, the lower two panels show how complicated the tube displacement eigenfunction becomes when the near fields of the two tubes are in communication. Also, it is important to note that the displacement amplitudes in the strong interaction case are larger by a factor of 10 or more than the isolated body counterpart. This aspect underscores the very premise of multiple scattering.

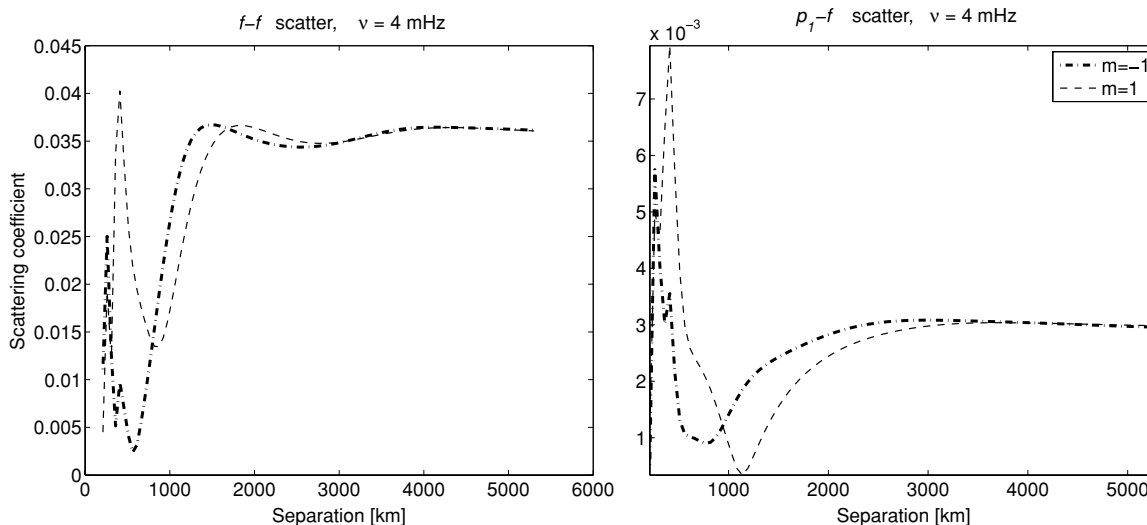


**Figure 6.** Scattering coefficients of the  $\beta = 1$  tube for an interacting pair of nonidentical  $\beta = 0.1, 1$  tubes. The behavior is unremarkable, not greatly differing from that in Figure 3. Note that because the magnetic flux in the tube is held constant, changes in  $\beta$  necessarily imply a change in flux tube radius. The incident  $f$  and  $p_1$  modes have horizontal wavelengths of 2.76 and 6.44 Mm, respectively.

scale height), tube merging, differences in the radiative transfer, etc. Moreover, it is a nontrivial task to compute the near field; this is further compounded by the uncertainties discussed in the first two paragraphs of this section. Solving the ideal magneto-hydrodynamic equations numerically may be the only way to study this problem in its full complexity.

### 5. CONCLUSIONS

The work of Bogdan & Zweibel (1987) was among the first efforts to characterize and study the multiple scattering of waves by flux tubes. Since then, further activity in this area was restricted to the study of multiple scattering by unstratified flux

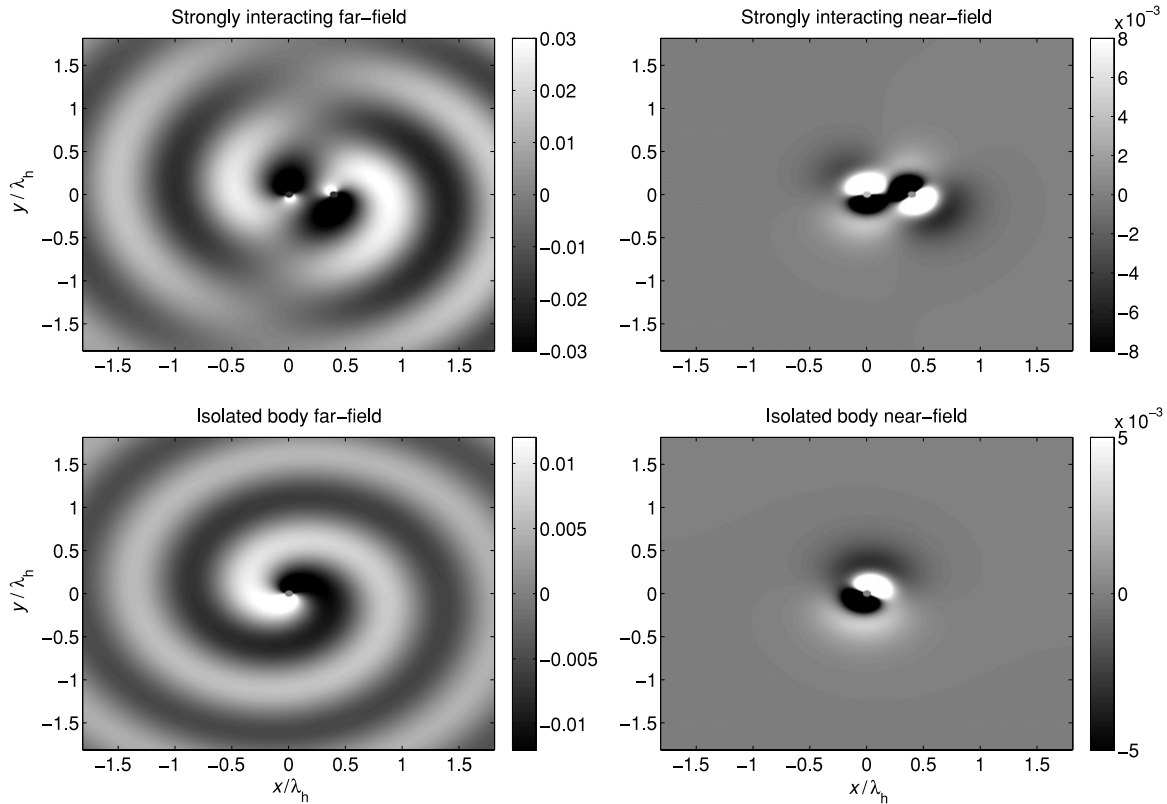


**Figure 7.** Real parts of the near and far scattered wave fields shown pictorially for a pair of  $\beta = 1$  flux tubes (upper panels) and the isolated body case (lower panels), both systems lit up by an incident 4 mHz  $f$  mode. The axes are  $x/\lambda_h$ ,  $y/\lambda_h$ , where  $\lambda_h$  is the horizontal wavelength of the incident  $f$  mode, 2.76 Mm. The far field is seen to spiral out whereas the near field is bound to within a distance of  $\lambda_h/2$  of the scatterer. Both fields pulsate with a period of 4.16 minutes (4 mHz wave). The tubes are separated by a distance of 1.085 Mm in the upper panels. There may be hope of observationally deducing the near-field modes by studying the zero-time-lag wave-field autocorrelations and using this information to determine properties of the scatterer.

tubes (e.g., Bogdan & Fox 1991; Keppens et al. 1994) and subsequently, single scattering by gravitationally stratified tubes (e.g., Bogdan et al. 1996; Hanasoge et al. 2008). Including stratification when attempting to solve the full multiple scattering problem introduces manifold difficulties, especially without the right set of techniques. However, much progress in this regard and the availability of the technique of Kagemoto & Yue (e.g., 1986) have allowed us to attempt this problem.

There has been the general thinking that not only does gravity inhibit resonant absorption but may in fact prevent strong interactions between closely spaced flux tubes. The reason for this is the disparity in the depth structure between the eigenfunctions of external modes and the tube displacement; gravity introduces strong structural differences between these two quantities, almost certainly ruling out a strong and direct matching between the two. Thus, resonant absorption in stratified magnetized environments may be largely ruled out; but what about multiple scattering and spikes in scattering cross-sections and phases? Is the theory of single scattering sufficient to describe the interaction of waves with clustered magnetic elements in the Sun? Certainly not, as demonstrated in Section 4. Fairly dramatic changes in the scattering coefficients are observed at close separations, on the order of several hundred kilometers, not unlike the distances between flux tubes in plage. The fact that scatter by a pair nonidentical flux tubes also exhibits a similar trend (Figure 6) demonstrates the robustness of multiple scattering type interactions. The scattering coefficient is a proxy for the degree of absorption and mode mixing exhibited by the system; if nothing else, the jumps in the coefficients point to a loss of

coherence of the incident modes, introducing a mechanism for wave damping.

The coefficients behave in a quirky manner, rather similar to those obtained by Bogdan & Fox (1991). Thus, drawing out larger behavioral properties from these interactions is somewhat difficult without a more detailed search of the parameter space. Part of this quiriness may be attributed to the interference between the sizable numbers of modes competing in the excitation of the flux tubes. Through analyses of observations of thousands of small magnetic elements, Duvall et al. (2006) succeeded in estimating the detailed scattering properties of these features, concluding that the  $m = \pm 1$  waves couple quite strongly with the magnetic tubes. Subsequently, Hanasoge et al. (2008) modeled these measurements in the single scattering limit in an attempt to constrain properties of the average magnetic element. However, these elements consist of a number of thin flux tubes, the scattering presumably in the strongly interacting regime due to their proximity. Merely with two tubes at a sequence of separations, the scattering coefficients and phases display remarkably intricate behavior; extending this to a number of flux tubes at various random locations is arguably a difficult task.

The near field in Figure 7 still remains to be directly detected in observations. One possible route toward this goal is to look for statistically significant zero time lag cross-correlation signals in the vicinity of these small magnetic elements. This follows from the spatially stationary nature of the near-field modes; they merely pulse at the frequency of the incident wave in a thin envelop around the scatterer. However, it is unclear how to

use this information in a productive manner; evidently a greater understanding of these evanescent waves is needed.

The question relating to sunspot structure, as to whether one can expect to be able to helioseismically discern a monolith from a jelly fish, still shows promise, for it would appear that multiple scattering, despite the presence of strong gravitational stratification, still plays a major role. Our preliminary conclusions, derived from Figures 3 and 4 echo those of Keppens et al. (1994), who suggested that ensembles of flux tubes can absorb quite effectively, but not cause coherent phasing of the scattered waves.

This work represents a small first step toward comprehending the action of multiple scattering in stratified magnetized environments. Much work remains to be done in terms of characterizing and understanding the interactions of clusters of randomly located flux tubes and the impact on mode line widths and observations of scattering in plage.

The idea for this work occurred over conversations at the CSPA, Monash University, where S.M.H. was a visiting academic in 2008. Much of the computation was performed on the Stanford University solar group machines; thanks to Phil Scherrer for the use of these resources. Some part of this work was accomplished while S.M.H. was at Stanford, he acknowledges support from NASA grant HMI NAS5-02139.

## APPENDIX A

### THE T AND B MATRICES

The procedure outlined here is adapted from Kagemoto & Yue (1986). In order to construct  $\mathbf{T}_{il}$ , we have the following formula for each  $|m, m'| \leq 1, n$ :

$$(\mathbf{T}_{il})_{cd} = e^{i(m-m')\gamma_{il}} H_{m-m'}^{(1)}(k_n R_{il}) \quad (\text{A1})$$

for  $n \leq n_p$ , where  $c = 3n + m' + 2$  and  $d = 3n + m + 2$ , and

$$(\mathbf{T}_{il})_{cd} = e^{i(m-m')\gamma_{il}} (-1)^{m'-1} K_{m-m'}(k_n R_{il}) \quad (\text{A2})$$

for  $n > n_p$ , where  $c, d$  are as above. The means of constructing  $\mathbf{B}_j$  are as follows. For every tuplet ( $|m| \leq 1, n$ ) an incident wave with the appropriate eigenfunction and radial behavior of unit amplitude is chosen. If  $n \leq n_p$ , the incident mode is propagating and has a  $J_m(k_n^p r)$  type horizontal behavior, whereas if  $n > n_p$ , the horizontal part of the eigenfunction is given by  $I_m(k_n^f r)$ . For each incident mode, the scattering into all other modes (at constant frequency and  $m$ ) is computed. Having thus computed the amplitudes of all the scattered waves for each incident mode, we fill up the matrix  $\mathbf{B}_j$  as follows:

$$(\mathbf{B}_j)_{cd} = \beta_{n',n}^m, \quad (\text{A3})$$

where  $\beta$  is the scatter into the mode  $(m, n')$  by incident wave  $(m, n)$ . The indices are  $c = 3n' + m + 2, d = 3n + m + 2$ . We only

consider  $|m| \leq 1$  since the tube is insensitive to other azimuthal orders in this theory.

## APPENDIX B

### TRANSFORMATION OF THE INCIDENT WAVE FIELD

We use Graf's addition formula (e.g., Abramowitz & Stegun 1964):

$$J_m(k_n^p r_i) e^{im(\theta_i - \gamma_{ij})} = \sum_{d=-\infty}^{\infty} J_{m+d}(k_n^p R_{ij}) J_d(k_n^p r_j) e^{ip(\pi - \theta_j + \gamma_{ij})}. \quad (\text{B1})$$

An  $m = 0$  wave seen at the axis center of tube  $i$  produces the following components at flux tube  $l$  whose center is located at distance  $R_{il}$  (the  $m = [-1, 0, 1]$  waves):

$$(J_1(k_n R_{il}) e^{i\gamma_{il}} J_0(k_n R_{il}) J_{-1}(k_n R_{il}) e^{-i\gamma_{il}}). \quad (\text{B2})$$

Similarly  $m = \pm 1$  waves seen at tube  $i$  produce at  $l$

$$(J_2(k_n R_{il}) e^{2i\gamma_{il}} J_1(k_n R_{il}) e^{i\gamma_{il}} J_0(k_n R_{il})), \quad (\text{B3})$$

$$(J_0(k_n R_{il}) J_{-1}(k_n R_{il}) e^{-i\gamma_{il}} J_{-2}(k_n R_{il}) e^{-2i\gamma_{il}}), \quad (\text{B4})$$

respectively. Since in our theory, the tube is insensitive to  $|m| > 1$ , we do not include these terms in the transformation.

## REFERENCES

- Abramowitz, M., & Stegun, I. A. 1964, Handbook of Mathematical Functions with Formulas, Graphs, and Mathematical Tables (9th ed.; New York: Dover) (10th ed. Washington: DCGPO)
- Barnes, G., & Cally, P. S. 2000, *Sol. Phys.*, **193**, 373
- Bogdan, T. J., & Cally, P. S. 1995, *ApJ*, **453**, 919
- Bogdan, T. J., & Fox, D. C. 1991, *ApJ*, **379**, 758
- Bogdan, T. J., Hindman, B. W., Cally, P. S., & Charbonneau, P. 1996, *ApJ*, **465**, 406
- Bogdan, T. J., & Zweibel, E. G. 1987, *ApJ*, **312**, 444
- Cameron, R., Gizon, L., & Daifallah, K. 2007, *Astron. Nachr.*, **328**, 313
- Duvall, T. L., Jr., A. C., Birch, & Gizon, L. 2006, *ApJ*, **646**, 553
- Duvall, T. L. J., D'Silva, S., Jefferies, S. M., Harvey, J. W., & Schou, J. 1996, *Nature*, **379**, 235
- Duvall, T. L., Jr., Jefferies, S. M., Harvey, J. W., & Pomerantz, M. A. 1993, *Nature*, **362**, 430
- Gizon, L., & Birch, A. C. 2004, *ApJ*, **614**, 472
- Gizon, L., Hanasoge, S. M., & Birch, A. C. 2006, *ApJ*, **643**, 549
- Hanasoge, S. M. 2008, *ApJ*, **680**, 1457
- Hanasoge, S. M., Birch, A. C., Bogdan, T. J., & Gizon, L. 2008, *ApJ*, **680**, 774
- Hindman, B. W., & Jain, R. 2008, *ApJ*, **677**, 769
- Kagemoto, H., & Yue, D. K. P. 1986, *J. Fluid Mech.*, **166**, 189
- Keppens, R., Bogdan, T. J., & Goossens, M. 1994, *ApJ*, **436**, 372
- Khomenko, E., & Collados, M. 2006, *ApJ*, **653**, 739
- Linton, C. M., & Evans, D. V. 1990, *J. Fluid Mech.*, **215**, 549
- Whittaker, E. T., & Watson, G. N. 1963, A Course of Modern Analysis (4th ed.; Cambridge: Cambridge Univ. Press)